Journal of Alloys and Compounds 815 (2020) 152375

Contents lists available at ScienceDirect

Journal of Alloys and Compounds

journal homepage: http://www.elsevier.com/locate/jalcom

Synthesis of Multilayer $InSe_{0.82}Te_{0.18}$ alloy for high performance near-infrared photodetector

Miaomiao Yu [a,1], Hang Li [b,1], Feng Gao [c], Yunxia Hu [c], Lifeng Wang [d], PingAn Hu [c,**], Wei Feng [a,*]

[a] College of Chemistry, Chemical Engineering and Resource Utilization, Northeast Forestry University, Harbin, 150040, China
[b] Innovation Lab of Space Robot System, Space Robotics Engineering Center, Changchun Institute of Optics, Fine Mechanics and Physics, Chinese Academy of Sciences, Changchun, 130033, China
[c] Key Lab of Microsystem and Microstructure of Ministry of Education, Harbin Institute of Technology, Harbin, 150080, China
[d] Institute for Frontier Materials, Deakin University, 75 Pigdons Road, Waurn Ponds, Geelong, Victoria, 3216, Australia

ARTICLE INFO

Article history:
Received 18 July 2019
Received in revised form
18 September 2019
Accepted 20 September 2019
Available online 20 September 2019

Keywords:
InSe
$InSe_{1-x}Te_x$
Alloy engineering
Photodetector
III-VI group semiconductors

ABSTRACT

Multilayer InSe has attracted increasing attention due to its excellent electrical and optical properties, making it great potential application in high performance electronic and optoelectronic devices. Alloy engineering is a powerful method to tune electrical and optical properties of semiconductors. However, the alloy engineering has never been applied to multilayer InSe. In this work, for the first time, multilayer $InSe_{0.82}Te_{0.18}$ alloy photodetector was fabricated and the photodetection performance of multilayer $InSe_{0.82}Te_{0.18}$ alloy was investigated. Compared to multilayer InSe, the multilayer $InSe_{0.82}Te_{0.18}$ alloy shows a broader photoresponse region of 400−1100 nm, which is due to its smaller direct bandgap of 1.13 eV. The $InSe_{0.82}Te_{0.18}$ alloy photodetector exhibits higher photodetection performance than InSe device and the responsivity (R) values are significantly enhanced by 50−300 times, especially in near-infrared (NIR) light region. The R value is 7.1 A/W for 1100 nm light, which surpasses most of multi-layer layered semiconductors based NIR photodetector. Moreover, the $InSe_{0.82}Te_{0.18}$ alloy photodetector owns a good photoresponse stability and relatively fast response time. This work demonstrates that $InSe_{0.82}Te_{0.18}$ alloy has a great potential application in NIR photodetector.

1. Introduction

Photodetector has attracted a significant attention due to its wide applications in imaging, sensor, communication and health monitoring [1–6]. For developing high performance of photodetector, various types of materials have been discovered. The rise of two-dimensional (2D) and thin-film materials has provided more options for designing novel and high performance photodetection devices. Most attentions have been focused on black phosphorous (BP) [7] and transition metal dichalcogenides (TMDs) [8–10]. However, instability hinders BP potential application and TMDs show narrow detection range due to their large bandgaps. Indium selenide (InSe), an interesting III-VI group layered semiconductor, has attracted increasing attention due to its excellent optical and electrical properties [11–17]. Because of its small bandgap (1.26 eV) and high absorption coefficient, photodetector based on few-layered InSe show a broad photoresponse to visible to NIR region (450–785 nm) and high photoresponsivity [14]. The photodetection performance can be effectively regulated by optimizing channel thickness [18] and contact electrode [19], and the responsivity increases to 10^5 A/W for graphene-InSe-graphene device illuminated by 633 nm laser [19]. Those result demonstrate that InSe is good candidate for high performance optoelectronic devices, such as photodetector and photodiode. Indium telluride (InTe), an important member of III-VI group family with a small direct bandgap [20], has been limited. Up to now, there is no experimental studies on 2D or multilayer InTe [21]. Theory calculation demonstrates that InSe–InTe heterostructure is a good candidate for solar cell and light emission applications [22].

Alloy engineering is an important and effective tool to adjust energy band structure, optical and electrical properties of materials, and has successfully been applied in modern semiconductor

* Corresponding author.
** Corresponding author.
E-mail addresses: hupa@hit.edu.cn (P. Hu), wfeng@nefu.edu.cn (W. Feng).
[1] M. Yu and H. Li contributed equally to this work.

https://doi.org/10.1016/j.jallcom.2019.152375
0925-8388/

field. Recently, alloy engineering also has been applied to 2D layered TMDs system [23–26] and photoresponse of TMDs alloys is significantly improved by alloy engineering due to shifting the deep-level defect states to shallow-level defect states [25]. Compared to TMDs system, alloy engineering is limited for investigation of optoelectronic and electrical properties of InSe-based alloy materials [27,28]. Though the tunable optical bandgaps of $InSe_{1-x}S_x$ ($x \le 0.3$) alloys [24] and superior second harmonic generation (SHG) performance in $InSe_{0.9}Te_{0.1}$ and $InSe_{1-x}S_x$ ($x = 0.1$ and 0.2) alloys [28] have been demonstrated, the study on optoelectronic properties of InSe-based alloys is still absent. The improvement photoresponse of transition metal dichalcogenides (TMDs) by alloy engineering is attributed to suppression of deep-level defect states [25]. 2D $Ga_{0.84}In_{0.16}Se$ alloy photodetector show superior performance than 2D GaSe photodetector for detecting visible light [29]. Those studies suggest that alloy engineering holds great potential in enhancing photodetection performance of multilayer InSe device and it is of interest to explore optoelectronic properties of $InSe_{1-x}Te_x$ alloys.

In this work, for the first time, we fabricated multilayer $InSe_{0.82}Te_{0.18}$ alloy photodetector and studied the photodetection performance of multilayer $InSe_{0.82}Te_{0.18}$ alloy. The multilayer $InSe_{0.82}Te_{0.18}$ alloy shows a broader photoresponse region of 400–1100 nm than that of multilayer InSe device, which is due to its smaller direct bandgap of 1.13 eV. The multilayer $InSe_{0.82}Te_{0.18}$ alloy photodetector shows a higher photodetection performance than InSe device and the R values are significantly enhanced by 50–300 times, especially in NIR light region. Moreover, the multilayer $InSe_{0.82}Te_{0.18}$ alloy photodetector shows a good photoresponse stability and fast photoresponse time. This work suggests that $InSe_{0.82}Te_{0.18}$ alloy is a potential material for application in NIR photodetector.

2. Experimental methods

2.1. Synthesis of bulk $InSe_{0.82}Te_{0.18}$ alloy

Bulk $InSe_{0.82}Te_{0.18}$ crystals were prepared by the following procedure: Indium (114.8 mg, 99.99%, Aladdin) (0.001 mol) and selenium-tellurium mixture (97 mg, 71.1% Se and 28.9% Te by weight, 99.99%, Alfa) were put in quartz boat, respectively. Then the boat was placed into a one-zone horizontal furnace with a fused silica tube. The close system was purged with 300 sccm Ar gas for 30 min. Firstly, the boat was heated to 573 K and kept at 573 K for 1 h with 100 sccm Ar/H_2 (V_{Ar}: $V_{H2} = 80:20$) as protection gas. Secondly, the boat was heated to 943 K and kept at 943 K for 1 h. Last, the system was naturally cooled to room temperature.

2.2. Characterizations of $InSe_{0.82}Te_{0.18}$ alloy

X-ray diffraction (XRD, DIFFRACTOMETER-6000) pattern was recorded with a Cu Kα radiation source ($\lambda = 0.1542$ nm). The chemical compositions of $InSe_{0.82}Te_{0.18}$ were determined by energy dispersive X-ray spectroscopy (EDS) (S-4200 Hitachi). The microstructures of $InSe_{0.82}Te_{0.18}$ were measured by transmission electron microscopy (TEM) and selected area electron diffraction (SAED), (FEITECNAI High Resolution TEM operated at 200 kV). The $InSe_{0.82}Te_{0.18}$ nanoflakes were transferred to lacey support films for the TEM tests by ultrasound in ethanol. The absorption spectrum of the alloy was obtained via a UV–vis–NIR spectrophotometer (UV3600, Shimadzu). Optical images of $InSe_{0.82}Te_{0.18}$ nanoflakes were taken with an OLYMPUS BX41. The thickness of multilayer $InSe_{0.82}Te_{0.18}$ was determined using atomic force microscopy (AFM, Nanoscope IIIa Vecco).

2.3. Fabrication and characterizations of InSe and $InSe_{0.82}Te_{0.18}$ alloy photodetectors

Multilayer InSe and $InSe_{0.82}Te_{0.18}$ nanosheets were mechanically exfoliated using Scotch tape and transferred onto 300 nm SiO_2/Si substrates. Metal electrodes (Cr = 5 nm, Au = 30 nm) were fabricated by thermal evaporation deposition with a shadow mask. Optoelectronic characterizations of multilayer InSe and $InSe_{0.82}Te_{0.18}$ nanosheets were measured using a semiconductor characterization system (Keithley 4200 SCS) with a Lakeshore probe station. Monochromatic lights of 400 nm, 500 nm, 600 nm, 700 nm, 800 nm, 900 nm, 1000 nm and 1100 nm were obtained using a 200 W xenon lamp with optical filters. The intensities of incident light source were determined by a power and energy meter (Model 372, Scienteck).

3. Results and discussions

The synthesized process of bulk $InSe_{1-x}Te_x$ alloy was described in experimental methods. Firstly, the crystal structure of as-synthesized bulk crystal was identified by X-ray diffraction (XRD) as shown in Fig. 1a. The main peaks are consistent with standard date file PDF#34–1341, which is hexagonal structure of InSe. The other minor peaks shown in XRD pattern are belonged to InTe [28]. The XRD pattern agrees well with early report of $InSe_{1-x}Te_x$ alloy, demonstrating that bulk $InSe_{1-x}Te_x$ alloy is successfully synthesized. To determine the element distribution and constituent of as-synthesized $InSe_{1-x}Te_x$ alloy, element mapping and X-ray energy-dispersive spectrum (EDS) were measured. Fig. 1b is a scanning electron microscopy (SEM) image and element mapping of as-synthesized $InSe_{1-x}Te_x$ alloy nanosheet. It clearly shows that three elements of In, Se and Te are homogeneously distributed over the selected nanosheet. The composition ratio of three elements (In:Se:Te) is 50.59:40.78:8.63, suggesting that as-synthesized alloy is $InSe_{0.82}Te_{0.18}$. The microstructure of $InSe_{0.82}Te_{0.18}$ alloy is examined by transmission electron microscopy (TEM). A good crystallinity of as-synthesized $InSe_{1-x}Te_x$ alloy is demonstrated by the selected area electron diffraction pattern (SAED) as shown in Fig. 1d inset. The good crystallinity is further demonstrated by high resolution transmission electron microscopy (HRTEM) as shown in Fig. 1d. The as-synthesized $InSe_{1-x}Te_x$ alloy shows a high crystallinity with a lattice spacing of 3.5 Å in Fig. 1d, which is slightly larger than 0.34 nm of InSe [13].

Alloy engineering is a powerful way to tune optical property of semiconductors [23]. It is of great importance to investigate optical property of $InSe_{0.82}Te_{0.18}$ alloy for its application in optoelectronic devices. The UV–Vis–NIR absorption spectra of InSe and $InSe_{0.82}Te_{0.18}$ alloy were measured and were shown in Fig. 2a. InSe has a wide optical absorption region from UV to NIR (300–1000 nm), which agrees well with its direct bandgap (E_g) of 1.26 eV. Compared to InSe, $InSe_{0.82}Te_{0.18}$ alloy shows a broader optical absorption spectrum from 300 to 1150 nm, indicating the alloy owns a smaller E_g value and broader photodetection range than InSe. To further quantitatively compare their E_g values, corresponding Tauc plots are exhibited in Fig. 2b. By extrapolating the linear part of Tauc plots, the optical E_g values of InSe and $InSe_{0.82}Te_{0.18}$ alloy are calculated to be 1.25 and 1.13 eV, respectively (find more calculated details in supporting information). The E_g value of $InSe_{0.82}Te_{0.18}$ alloy takes a blue shift of 0.12 eV in contrast with InSe. The optical absorption results of InSe and $InSe_{0.82}Te_{0.18}$ alloy demonstrate that alloy engineering is an efficient tool to adjust optical properties of InSe and $InSe_{0.82}Te_{0.18}$ alloy holds a great potential application in optoelectronic devices.

To investigate photoresponse performance of $InSe_{0.82}Te_{0.18}$ alloy, the photodetector based on multilayer $InSe_{0.82}Te_{0.18}$ alloy was

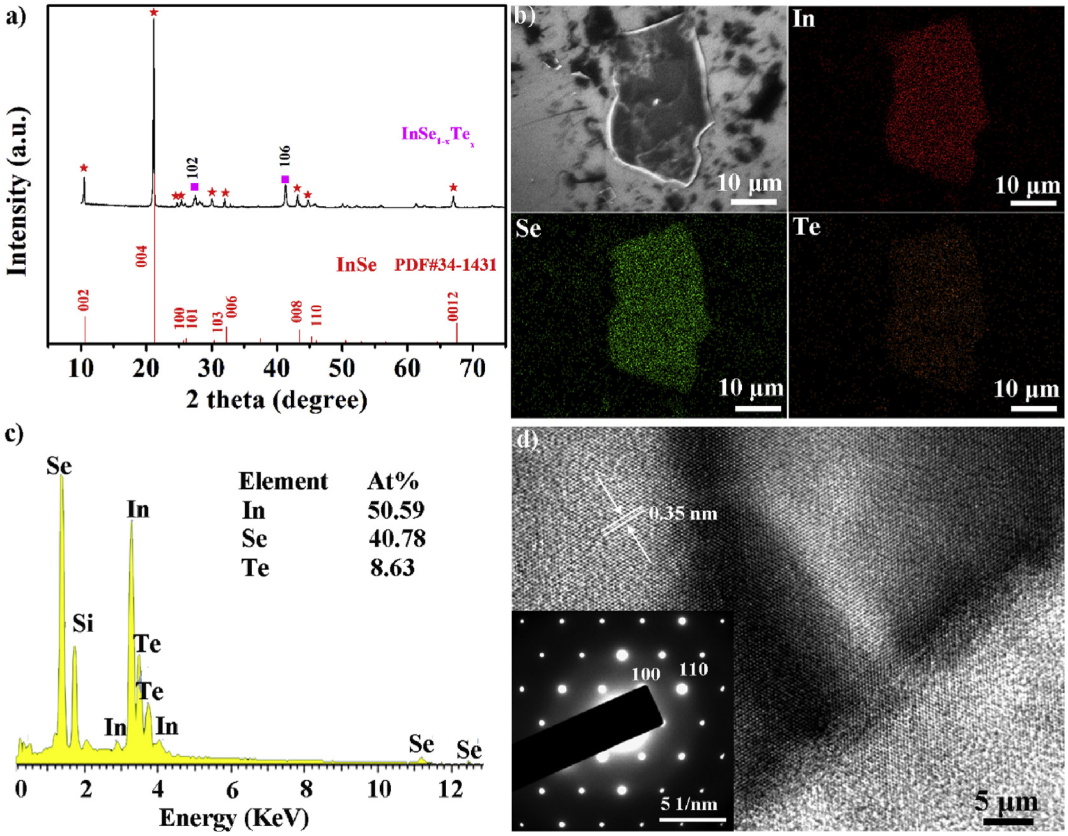

Fig. 1. Crystalline structure characterization of $InSe_{1-x}Te_x$ (x = 0.18) alloy: (a) XRD pattern of $InSe_{1-x}Te_x$ alloy. (b) Element mapping image of $InSe_{1-x}Te_x$ alloy. (c) EDS image of $InSe_{1-x}Te_x$ alloy. (d) HRTEM image of $InSe_{1-x}Te_x$ alloy. Inset: the corresponding reverse Fourier transform pattern. Inset: SAED pattern of $InSe_{1-x}Te_x$ alloy.

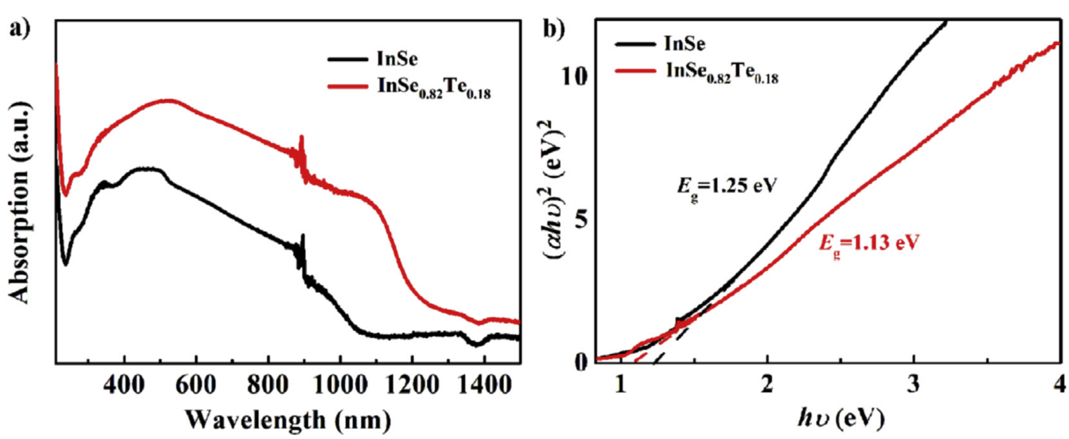

Fig. 2. Optical absorption properties: (a) UV–Vis–NIR absorption spectra of InSe and $InSe_{0.82}Te_{0.18}$ alloy. (b) The corresponding Tauc plots of InSe and $InSe_{0.82}Te_{0.18}$ alloy.

fabricated (find more fabrication details in Experimental methods). Fig. 3a is the 3D schematic structure of $InSe_{0.82}Te_{0.18}$ alloy photodetector. The electrodes are Au/Cr (35 nm/5 nm) and various lights with tunable intensities are vertically illuminated on device. Fig. 3b is an optical image of $InSe_{0.82}Te_{0.18}$ alloy photodetector and the device channel length and width are 20 and 10 μm, respectively, and the light active area of photodetector is calculated to be 200 μm^2. The device channel thickness is around 60 nm, which is determined by atomic force microscope (AFM) in Fig. S1. Fig. S2 is the transfer curve of multilayer $InSe_{0.82}Te_{0.18}$ transistor, demonstrating multilayer $InSe_{0.82}Te_{0.18}$ is a p-type semiconductor with a mobility of 4.5 $cm^2\,V^{-1}s^{-1}$ (find more discussion in Supporting Information). The I–V curves of $InSe_{0.82}Te_{0.18}$ alloy photodetector illuminated by various lights were recorded and are shown in Fig. 3c. The $InSe_{0.82}Te_{0.18}$ alloy photodetector shows a wide photoresponse range from visible (400 nm) to NIR light (1100 nm), which is consistent with its optical absorption. To compare photodetection performance of InSe and $InSe_{0.82}Te_{0.18}$ alloy, multilayer InSe photodetector was fabricated and illumination I–V curves are displayed in Fig. S3. InSe photodetector shows a photoresponse range from visible (400 nm) to NIR light (1000 nm), which is consistent with earlier report [30].

To quantitatively evaluate photoresponse of InSe and $InSe_{0.82}Te_{0.18}$ alloy photodetectors, responsivity (R) and detectivity

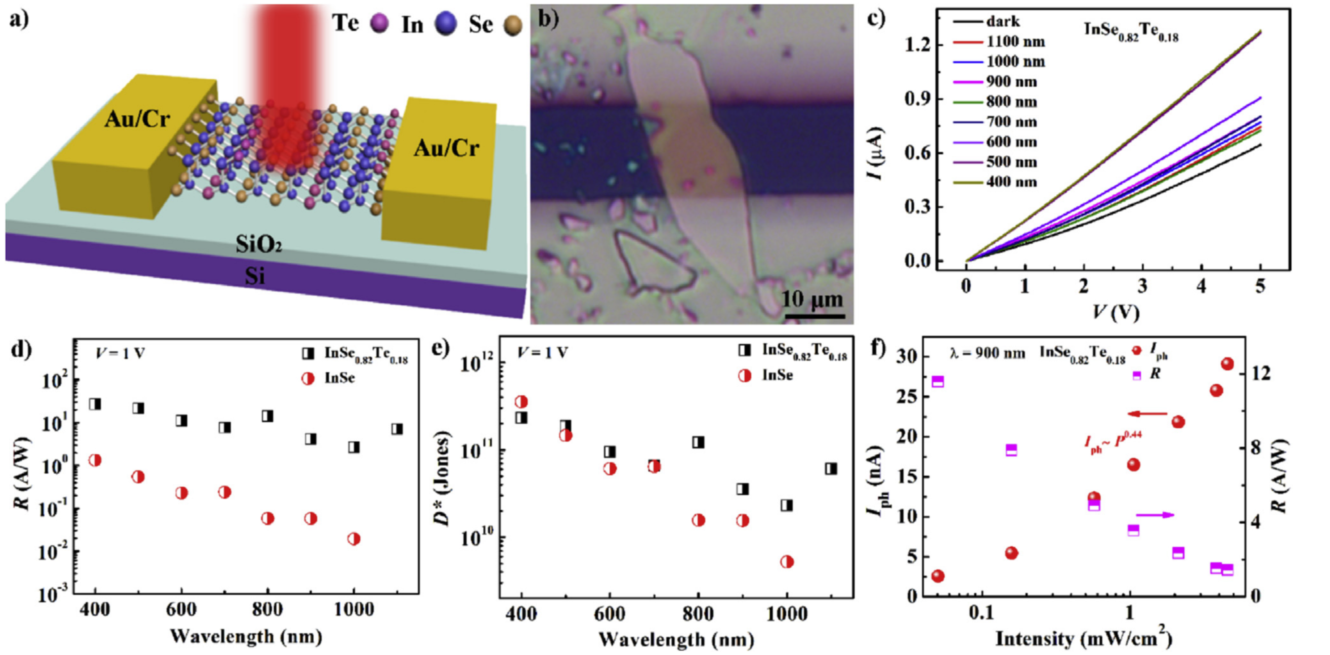

Fig. 3. Photoresponse performance of multilayer $InSe_{0.82}Te_{0.18}$ alloy. (a) 3D schematic structure of alloy $InSe_{0.82}Te_{0.18}$ photodetector. (b) A typical optical image of alloy $InSe_{0.82}Te_{0.18}$ photodetector. (c) *I*–*V* curves of the multilayer $InSe_{0.82}Te_{0.18}$ alloy photodetector illuminated at different wavelengths. The illumination intensities are 2.16 mW/cm^2, 2.61 mW/cm^2, 2.11 mW/cm^2, 1.46 mW/cm^2, 0.438 mW/cm^2, 3.83 mW/cm^2, 4.29 mW/cm^2 and 0.924 mW/cm^2 for 400, 500, 600, 700, 800, 900, 1000 and 1100 nm, respectively. (d) *R* values and (e) D^* values of InSe and $InSe_{0.82}Te_{0.18}$ alloy photodetector for various wavelengths at $V = 1$ V. (f) I_{ph} and *R* values of $InSe_{0.82}Te_{0.18}$ alloy photodetector illuminated at 900 nm and $V = 1$ V with various light intensities.

(D^*) are calculated (find more detailed calculation in supporting information), which are two important parameters for a photodetector. The calculated *R* values of InSe and $InSe_{0.82}Te_{0.18}$ alloy photodetectors illuminated by various lights with a bias of 1 V are shown in Fig. 3d. The $InSe_{0.82}Te_{0.18}$ alloy photodetector shows higher *R* values than those of InSe photodetector in whole illumination range. For example, the *R* value is 2.7 A/W and 7.1 A/W for $InSe_{0.82}Te_{0.18}$ alloy photodetector under 1000 nm and 1100 nm, which is two order of magnitudes higher than 0.02 A/W (1000 nm) of InSe photodetector. The *R* value is effectively increased by 50–300 times in illumination region of 400–1000 nm by alloy engineering. And the alloy photodetector has a response to 1100 nm light, which slightly expands the photodetection range. The *R* value strongly depends on applied bias as shown in Fig. S4a and the *R* increases as applied bias increases. This behavior is attributed to shortening of the carriers' transit time and reduction of the possibility of recombination by larger bias, which lead to higher photocurrent [14]. For 1100 nm light, the *R* increases to 47.4 A/W at a bias of 5 V. Compared to InSe photodetector, the D^* values of $InSe_{0.82}Te_{0.18}$ alloy photodetector are slightly enhanced in Fig. 3e, which are in the range of 10^{10}-10^{11} Jones. The external quantum efficiency (EQE) of $InSe_{0.82}Te_{0.18}$ alloy photodetectors is 1–2 orders of magnitude higher than that of InSe photodetectors as shown in Fig. S4b (find detailed calculation in Supporting Information). The I_{ph}/I_{dark} is another important feature of merit for a photodetector. The I_{ph}/I_{dark} is 1.4 and 66 for $InSe_{0.82}Te_{0.18}$ alloy and InSe photodetector for 400 nm light, respectively. Compared to multilayer InSe photodetector, lower I_{ph}/I_{dark} for multilayer $InSe_{0.82}Te_{0.18}$ photodetector is limited by the high dark current, thus leaving room for future improvement. As shown in Table S1, the $InSe_{0.82}Te_{0.18}$ alloy photodetector shows a good NIR detection performance, which surpasses most of multilayer layered semiconductors [21–33], such as BP, GeSe and Bi_2O_2Se. The alloy photodetector was illuminated by 900 nm with various light intensities and the calculated photocurrent (I_{ph}) and *R* values at a bias of 1 V are exhibited in Fig. 3f. The I_{ph} increases as light intensity increases, which is directly proportional to $P^{0.44}$, suggesting that part of photogenerated carriers recombine through trap states. The *R* values decrease as light intensity increases, owing to trap states in either in $InSe_{0.82}Te_{0.18}$ alloy nanosheets or at the interface between the $InSe_{0.82}Te_{0.18}$ alloy and SiO_2 substrate, which are similar to InSe photodetector [18]. Above results demonstrate that photoresponse of InSe is significantly enhanced by alloy engineering, and $InSe_{0.82}Te_{0.18}$ alloy photodetector owns a broadband photoresponse region from visible (400 nm) to NIR light (1100 nm).

The stability is an important parameter to a photodetector in practical application. To investigate the stability of $InSe_{0.82}Te_{0.18}$ alloy photodetector, modulated 900 nm light were illuminated on this device and the current is shown in Fig. 4a. The photodetector shows a good multi-cycles stability with a reproduced switching from light-on to light-off state. Response time is another important parameter for a photodetector to applied in optical communication. To extract dynamic response time of rise process and decay process, a magnified photoresponse curve is shown in Fig. 4b. The response time is 1 and 3 s for rise process and decay process, respectively. The response speed of alloy photodetector is slower than InSe photodetector [14], which may be due to defects derived from the process of Te replacing Se.

4. Conclusions

In summary, the multilayer $InSe_{0.82}Te_{0.18}$ alloy photodetector was fabricated and the photoresponse of multilayer $InSe_{0.82}Te_{0.18}$ alloy was studied for the first time. Compared to multilayer InSe, the multilayer $InSe_{0.82}Te_{0.18}$ alloy shows a broader photoresponse from visible light (400 nm) to NIR light (1100 nm), which is due to its smaller direct bandgap of 1.13 eV. The multilayer $InSe_{0.82}Te_{0.18}$ alloy photodetector exhibits higher photodetection performance

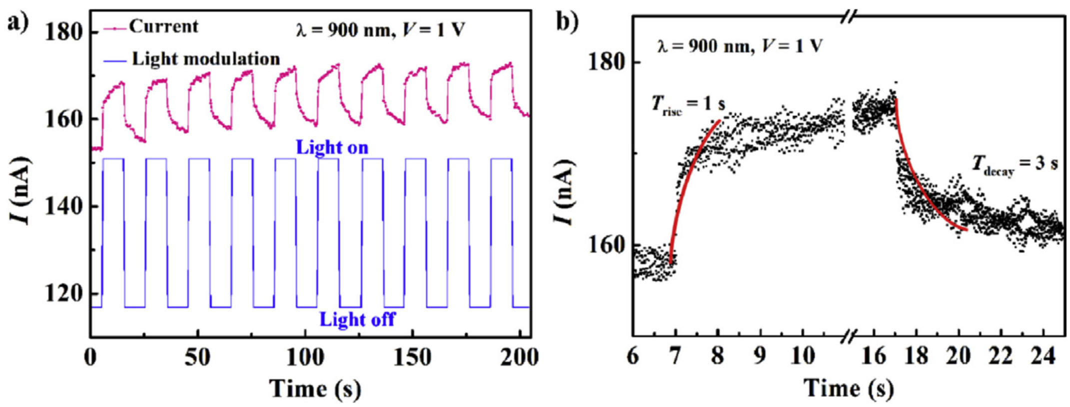

Fig. 4. Stability of $InSe_{0.82}Te_{0.18}$ alloy photodetector. (a) Time-dependent photoresponse stability of $InSe_{0.82}Te_{0.18}$ photodetectors illuminated by 900 nm light at $V = 1$ V with an illumination intensity of 3.83 mW/cm^2. (b) Corresponding response time.

than InSe device and the R values are significantly enhanced by 50–300 times, especially in NIR light region. The R value is 7.1 A/W for 1100 nm light, which surpasses most of multilayer layered semiconductors, such as BP, GeSe and Bi_2O_2Se. Besides, the multilayer $InSe_{0.82}Te_{0.18}$ alloy photodetector owns a good stability and relatively fast response time. This work demonstrates that alloy engineering is powerful tool to improve photoresponse of multilayer InSe and suggests that $InSe_{0.82}Te_{0.18}$ alloy is a good candidate for application in NIR photodetector.

Associated content

Notes

The authors declare no any competing financial interest.

Acknowledgment

We gratefully acknowledge the support from the National Natural Science Foundation of China (NSFC, No. 51802038), the China Postdoctoral Science Foundation (No. 2019T120246, 2018M630329) and Heilongjiang Postdoctoral Special Fund (No. LBH-TZ1801).

Appendix A. Supplementary data

Supplementary data to this article can be found online at https://doi.org/10.1016/j.jallcom.2019.152375.

References

[1] R.H. Dyck, G.P. Weckler, Integrated arrays of silicon photodetectors for image sensing, IEEE Trans. Electron Devices 15 (1968) 196–201.
[2] H. Melchior, M.B. Fisher, F.R. Arams, Photodetectors for optical communication systems, Proc. IEEE 58 (1970) 1466–1486.
[3] T. Mueller, F. Xia, P. Avouris, Graphene photodetectors for high-speed optical communications, Nat. Photonics 4 (2010) 297.
[4] D. Guo, Y. Su, H. Shi, P. Li, N. Zhao, J. Ye, S. Wang, A. Liu, Z. Chen, C. Li, W. Tang, Self-powered ultraviolet photodetector with superhigh photoresponsivity (3.05 A/W) based on the GaN/Sn:Ga_2O_3 pn junction, ACS Nano 12 (2018) 12827–12835.
[5] D. Guo, H. Liu, P. Li, Z. Wu, S. Wang, C. Cui, C. Li, W. Tang, Zero-power-consumption solar-blind photodetector based on β-Ga_2O_3/NSTO heterojunction, ACS Appl. Mater. Interfaces 9 (2017) 1619–1628.
[6] D.Y. Guo, H.Z. Shi, Y.P. Qian, M. Lv, P.G. Li, Y.L. Su, Q. Liu, K. Chen, S.L. Wang, C. Cui, C.R. Li, W.H. Tang, Fabrication of β-Ga_2O_3/ZnO heterojunction for solar-blind deep ultraviolet photodetection, Semicond. Sci. Technol. 32 (2017), 03LT01.
[7] M. Huang, M. Wang, C. Chen, Z. Ma, X. Li, J. Han, Y. Wu, Broadband black-phosphorus photodetectors with high responsivity, Adv. Mater. 28 (2016) 3481–3485.
[8] Z. Yin, H. Li, H. Li, L. Jiang, Y. Shi, Y. Sun, G. Lu, Q. Zhang, X. Chen, H. Zhang, Single-layer MoS_2 phototransistors, ACS Nano 6 (2012) 74–80.
[9] W. Choi, M.Y. Cho, A. Konar, J.H. Lee, G.-B. Cha, S.C. Hong, S. Kim, J. Kim, D. Jena, J. Joo, S. Kim, High-detectivity multilayer MoS_2 phototransistors with spectral response from ultraviolet to infrared, Adv. Mater. 24 (2012) 5832–5836.
[10] H. Tan, Y. Fan, Y. Zhou, Q. Chen, W. Xu, J.H. Warner, Ultrathin 2D photodetectors utilizing chemical vapor deposition grown WS_2 with graphene electrodes, ACS Nano 10 (2016) 7866–7873.
[11] G.W. Mudd, S.A. Svatek, T. Ren, A. Patanè, O. Makarovsky, L. Eaves, P.H. Beton, Z.D. Kovalyuk, G.V. Lashkarev, Z.R. Kudrynskyi, A.I. Dmitriev, Tuning the bandgap of exfoliated InSe nanosheets by quantum confinement, Adv. Mater. 25 (2013) 5714–5718.
[12] S. Lei, L. Ge, S. Najmaei, A. George, R. Kappera, J. Lou, M. Chhowalla, H. Yamaguchi, G. Gupta, R. Vajtai, A.D. Mohite, P.M. Ajayan, Evolution of the electronic band structure and efficient photo-detection in atomic layers of InSe, ACS Nano 8 (2014) 1263–1272.
[13] W. Feng, W. Zheng, W. Cao, P. Hu, Back gated multilayer InSe transistors with enhanced carrier mobilities via the suppression of carrier scattering from a dielectric interface, Adv. Mater. 26 (2014) 6587–6593.
[14] S.R. Tamalampudi, Y.-Y. Lu, R. Kumar U, R. Sankar, C.-D. Liao, K. Moorthy B, C.-H. Cheng, F.C. Chou, Y.-T. Chen, High performance and bendable few-layered InSe photodetectors with broad spectral response, Nano Lett. 14 (2014) 2800–2806.
[15] S. Sucharitakul, N.J. Goble, U.R. Kumar, R. Sankar, Z.A. Bogorad, F.-C. Chou, Y.-T. Chen, X.P.A. Gao, Intrinsic electron mobility exceeding 10^3 cm$^{2/}$(Vs) in multilayer InSe FETs, Nano Lett. 15 (2015) 3815–3819.
[16] D.A. Bandurin, A.V. Tyurnina, G.L. Yu, A. Mishchenko, V. Zólyomi, S.V. Morozov, R.K. Kumar, R.V. Gorbachev, Z.R. Kudrynskyi, S. Pezzini, Z.D. Kovalyuk, U. Zeitler, K.S. Novoselov, A. Patanè, L. Eaves, I.V. Grigorieva, V.I. Fal'ko, A.K. Geim, Y. Cao, High electron mobility, quantum Hall effect and anomalous optical response in atomically thin InSe, Nat. Nanotechnol. 12 (2016) 223.
[17] A. Gao, J. Lai, Y. Wang, Z. Zhu, J. Zeng, G. Yu, N. Wang, W. Chen, T. Cao, W. Hu, D. Sun, X. Chen, F. Miao, Y. Shi, X. Wang, Observation of ballistic avalanche phenomena in nanoscale vertical InSe/BP heterostructures, Nat. Nanotechnol. 14 (2019) 217–222.
[18] W. Feng, J.-B. Wu, X. Li, W. Zheng, X. Zhou, K. Xiao, W. Cao, B. Yang, J.-C. Idrobo, L. Basile, W. Tian, P. Tan, P. Hu, Ultrahigh photo-responsivity and detectivity in multilayer InSe nanosheets phototransistors with broadband response, J. Mater. Chem. C 3 (2015) 7022–7028.
[19] G.W. Mudd, S.A. Svatek, L. Hague, O. Makarovsky, Z.R. Kudrynskyi, C.J. Mellor, P.H. Beton, L. Eaves, K.S. Novoselov, Z.D. Kovalyuk, E.E. Vdovin, A.J. Marsden, N.R. Wilson, A. Patanè, High broad-band photoresponsivity of mechanically formed InSe–graphene van der Waals heterostructures, Adv. Mater. 27 (2015) 3760–3766.
[20] S. Pal, D.N. Bose, Growth, characterisation and electrical anisotropy in layered chalcogenides GaTe and InTe, Solid State Commun. 97 (1996) 725–729.
[21] S. Demirci, N. Avazlı, E. Durgun, S. Cahangirov, Structural and electronic properties of monolayer group III monochalcogenides, Phys. Rev. B 95 (2017) 115409.
[22] J. Shang, L. Pan, X. Wang, J. Li, H.-X. Deng, Z. Wei, Tunable electronic and optical properties of InSe/InTe van der Waals heterostructures toward optoelectronic applications, J. Mater. Chem. C 6 (2018) 7201–7206.
[23] H. Li, X. Duan, X. Wu, X. Zhuang, H. Zhou, Q. Zhang, X. Zhu, W. Hu, P. Ren, P. Guo, L. Ma, X. Fan, X. Wang, J. Xu, A. Pan, X. Duan, Growth of alloy $MoS_{2x}Se_{2(1-x)}$ nanosheets with fully tunable chemical compositions and optical properties, J. Am. Chem. Soc. 136 (2014) 3756–3759.
[24] X. Duan, C. Wang, Z. Fan, G. Hao, L. Kou, U. Halim, H. Li, X. Wu, Y. Wang, J. Jiang, A. Pan, Y. Huang, R. Yu, X. Duan, Synthesis of $WS_{2x}se_{2-2x}$ alloy

nanosheets with composition-tunable electronic properties, Nano Lett. 16 (2016) 264–269.
[25] J. Yao, Z. Zheng, G. Yang, Promoting the performance of layered-material photodetectors by alloy engineering, ACS Appl. Mater. Interfaces 8 (2016) 12915–12924.
[26] Z. Zheng, J. Yao, G. Yang, Centimeter-scale deposition of $Mo_{0.5}W_{0.5}Se_2$ alloy film for high-performance photodetectors on versatile substrates, ACS Appl. Mater. Interfaces 9 (2017) 14920–14928.
[27] H. Li, X. Han, D. Pan, X. Yan, H.-W. Wang, C. Wu, G. Cheng, H. Zhang, S. Yang, B. Li, H. He, J. Wang, Bandgap engineering of InSe single crystals through S substitution, Cryst. Growth Des. 18 (2018) 2899–2904.
[28] Q. Hao, H. Yi, H. Su, B. Wei, Z. Wang, Z. Lao, Y. Chai, Z. Wang, C. Jin, J. Dai, W. Zhang, Phase identification and strong second harmonic generation in pure ε-InSe and its alloys, Nano Lett. 19 (2019) 2634–2640.
[29] M. Yu, H. Li, H. Liu, F. Qin, F. Gao, Y. Hu, M. Dai, L. Wang, W. Feng, P. Hu, Synthesis of two-dimensional alloy $Ga_{0.84}In_{0.16}Se$ nanosheets for high-performance photodetector, ACS Appl. Mater. Interfaces 10 (2018) 43299–43304.
[30] Z. Yang, W. Jie, C.-H. Mak, S. Lin, H. Lin, X. Yang, F. Yan, S.P. Lau, J. Hao, Wafer-scale synthesis of high-quality semiconducting two-dimensional layered InSe with broadband photoresponse, ACS Nano 11 (2017) 4225–4236.
[31] L. Li, W. Wang, L. Gan, N. Zhou, X. Zhu, Q. Zhang, H. Li, M. Tian, T. Zhai, Ternary Ta_2NiSe_5 flakes for a high-performance infrared photodetector, Adv. Funct. Mater. 26 (2016) 8281–8289.
[32] J. Li, Z. Wang, Y. Wen, J. Chu, L. Yin, R. Cheng, L. Lei, P. He, C. Jiang, L. Feng, J. He, High-performance near-infrared photodetector based on ultrathin Bi_2O_2Se nanosheets, Adv. Funct. Mater. 28 (2018) 1706437.
[33] N. Youngblood, C. Chen, S.J. Koester, M. Li, Waveguide-integrated black phosphorus photodetector with high responsivity and low dark current, Nat. Photonics 9 (2015) 247.